Comparisons of the Seismic Properties of the Sun During Solar Cycles 23 and 24

Scott Harmon, Trent Herdtner, William Jackson, Chris Lindsay, Morgan Lynn, David Nguyen, Shejuti Shahriar, Aagam Vadecha, Kyle Vorys, Haochen Wang
Advisors: Edward Rhodes, Stephen Pinkerton Department of Physics and Astronomy, University of Southern California
Collaborators: Sophia Singh, USC Dept. of Aerospace and Mechanical Engineering; Tim Larson, Stanford University; Johann Reiter, Technical University of Munich
Acknowledgement: Daniel Joo, Jonathan Kim, Samuel Lee, LAUSD

Abstract

The current solar activity cycle, Cycle 24, is weaker than the three previous cycles. Because of this relative weakness in the level of solar activity, we are interested in learning whether the seismic properties of the current solar atmosphere are different from those in Cycle 23. In order to answer this question, we first added another 1.8 years of solar data to the amount we had available last year. We then compared the changes in the frequencies of solar oscillations observed during Cycle 24 with simultaneous changes in seven different indicators of solar activity. We then repeated this analysis for all of Cycle 23 using 15 years of MDI oscillation data. We discovered that the sensitivity of the short-term frequency changes to long-term MgII activity changes is significantly reduced by 39 percent in Cycle 24 when compared with Cycle 23.

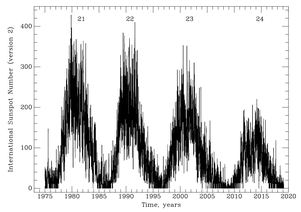

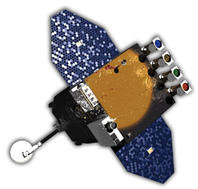

Figure 1: (a) (left): Temporal dependence of the mean International Sunspot Number for solar cycles 21–24 (to March, 2019)
(b) (right): Image of Solar Dynamics Observatory (Courtesy NASA/GSFC)

Purpose

Our project aims to study the continuing decline in average solar activity over Solar Cycles 23 to 24, as shown in Figure 1a. Understanding the changes in the Sun's acoustic oscillations will help predict future solar activity and by extension, solar flare activity and climate change.

Method

Our data comes from NASA's Helioseismic and Magnetic Imager (Figure 1b), Michelson Doppler Imager, and GONG+. A total of **1457** 3-day time series of dopplergrams were processed by the HMI team at Stanford University, where they were each converted into a set of un-averaged spectra. We transferred the un-averaged spectra to USC and collapsed each of those into a set of **1001** m-averaged spectra. We then fit the peaks in all of the m-averaged spectra from a single 3-day run with the latest version of our Windowed, Multi-Peak, Averaged Spectrum (WMLTP) peak-fitting technique, which fits a set of theoretical profiles to each of the peaks in each m-averaged spectrum. By applying this method to all of the m-averaged spectra from a single run, we obtained a total of **12 288** frequencies, such as those shown in Figure 2a. We also obtained the same number of linewidths, such as those shown in Figure 2b, and the same number of amplitudes, such as those shown in Figure 2c. We next split these tables of fitted parameters into **45** 72-day time intervals. We paired all **24** of the tables within each interval and subtracted the corresponding frequencies, linewidths, and amplitudes, generating a total of **276** sets of differences within each interval. One of these sets of frequency differences is shown in Figure 3a. We next binned each set of frequency, width, and amplitude differences into **25 250 μHz**-wide bins. The binned frequency shifts that resulted from the raw differences shown in Figure 3a are shown in Figure 3b.

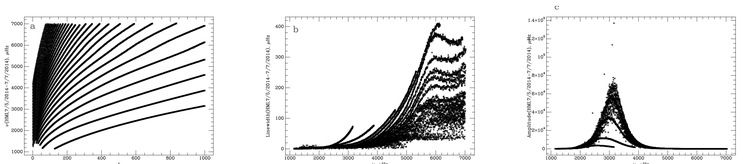

Figure 2: (a) (left): The **12 228** solar oscillation frequencies computed from the HMI observing run of July 5 to July 7, 2014, plotted as a function of the spherical harmonic degree.
(b) (center): The frequency dependence of the linewidths of the oscillations computed from the same run.
(c) (right): The frequency dependence of the amplitudes of the oscillations computed from the same run.

Data and Results

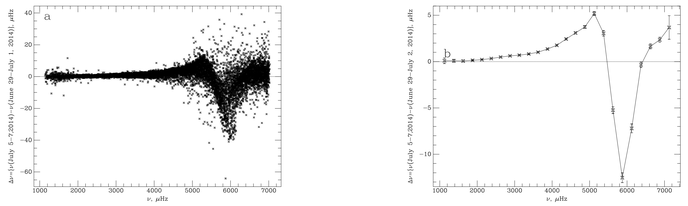

Figure 3: (a) (left): The frequency dependence of the **12 228** differences in the frequencies computed from the July 5 to July 7, 2014 run and the frequencies computed from the June 29 to July 1, 2014 run.
(b) (right): The frequency dependence of the **25** binned frequency differences computed from the raw frequency differences shown in panel a. Also shown are the standard errors of each mean frequency. The horizontal dotted line designates frequency differences of **0.0**.

We next regressed the **276** binned frequency shifts within each of our **25** bins against differences in 3-day averages of nine different solar activity indices. One example of these regressions for a frequency bin where the frequency shifts were correlated with the activity shifts is shown in Figure 4a. A second example from a higher-frequency bin where the frequency shifts were anti-correlated with the activity differences is shown in Figure 4b.

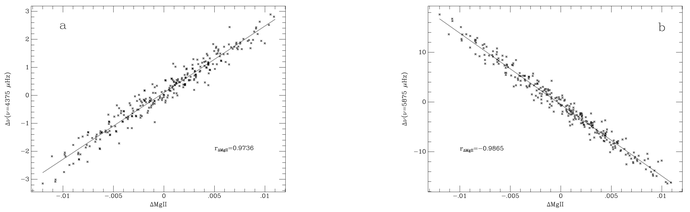

Figure 4: (a) (left): The dependence of the binned frequency differences in the bin centered at $\nu = 4375\,\mu\text{Hz}$ upon the Magnesium 2 Spectra Line (MgII) core-to-wing ratios. The solid line shows the linear regression fit to the **276** data points. The positive slope of this line shows that the frequencies were correlated with the changes in solar activity for this bin. The correlation coefficient $r = 0.9736$, shows that the correlation was strong.
(b) (right): The dependence of the binned frequency differences in the bin centered at $\nu = 5875\,\mu\text{Hz}$ upon the MgII core-to-wing ratios. The solid line is the linear regression fit to the 276 data points. The negative slope shows that the frequency were anti-correlated with the changes in solar activity for this bin. The correlation coefficient $r = -0.9865$, shows that the anti-correlation was also strong.

Previous studies of the frequency and linewidth shifts showed systematic signatures in both the slopes and correlation coefficients from similar regression analyses. The signature of the frequency shifts from the first 72-day time interval is shown in Figure 5a. At low frequencies the frequency shifts were correlated with the activity changes, while at intermediate frequencies they became anti-correlated, before once again becoming correlated with the activity changes. We defined the frequency at which the sign of the correlation coefficient changed from positive to negative as $\nu_{+/-}$ and the frequency where it changed back from negative to positive as $\nu_{-/+}$. We show examples of both of these zero-crossing frequencies in Figure 5a.

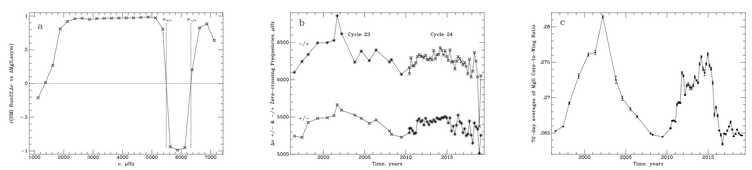

Figure 5: (a) (left): The frequency dependence of the correlation coefficients computed from the **25** linear regression analyses of the binned frequency differences upon the changes in MgII. The left-hand vertical dashed line shows the frequency at which the frequency shifts changed from being correlated with the activity changes to being anti-correlated. This frequency, $\nu_{+/-}$, is designated as the $+/-$ zero-crossing frequency. The right-hand vertical dashed line shows the frequency at which the frequency shifts returned to being positively correlated with the activity differences. This frequency, $\nu_{-/+}$, is designated as the $-/+$ zero-crossing frequency.
(b) (center): Plot of both $\nu_{+/-}$ and $\nu_{-/+}$ zero crossings as functions of time.
(c) (right): Plot of the 72 day averages of the MgII Core-to-Wing Ratio over time.

The results shown in Figure 5a illustrate the signatures of the short-term temporal variations on a scale of a few days. These short-term signatures were very similar in Cycles 23 and 24. However, we wanted to compare the long-term changes on the scale of an entire solar cycle. In order to search for such long-term variations, we repeated all of the above steps for 15 time intervals in Cycle 23 and 45 additional 72-day time intervals in Cycle 24. Both sets of the resulting zero-crossing frequencies are shown as functions of time during both cycles in Figure 5b. Also, the corresponding average values of the MgII Core-to-Wing Ratio solar activity index are shown as a function of time for both cycles in Figure 5c. In order to determine whether the longer-term changes in the frequencies were different in Cycles 23 and 24, we separated our tables of zero-crossings into two smaller tables. The first table contained our MDI zero-crossing frequencies from Cycle 23 (along with a few frequencies from GONG project data in 2001) and the second contained our 44 sets of HMI results from Cycle 24 and one set of MDI results from 2010. We next regressed all of the $+/-$ frequencies and all of the $-/+$ frequencies in the first table against the average values of the MgII index during each of the 15 observing runs. We then regressed all of the $+/-$ frequencies and all of the $-/+$ frequencies in the second table against the average values of the MgII index during each of those 45 observing runs. All four of these long-term regression fits are shown in the four panels of Figure 6. To test the statistical significance of the differences in the intercepts and slopes of our two pairs of regression fits, we employed the statistical tests described in **"Applied Regression Analysis and Other Multivariable Methods"** by Kleinbaum and Kupper (1978). We found that both the intercepts and the slopes of the two $-/+$ frequency regressions differed significantly at the 99 percent confidence level, while the intercepts and slopes of the two $+/-$ frequency regressions differed significantly at the 90 percent confidence level. For example, the $+/-$ slope in Cycle 24 was only **0.67** of the $+/-$ slope in Cycle 23, while the $-/+$ slope in Cycle 24 was only **0.54** of the $-/+$ slope in Cycle 23.

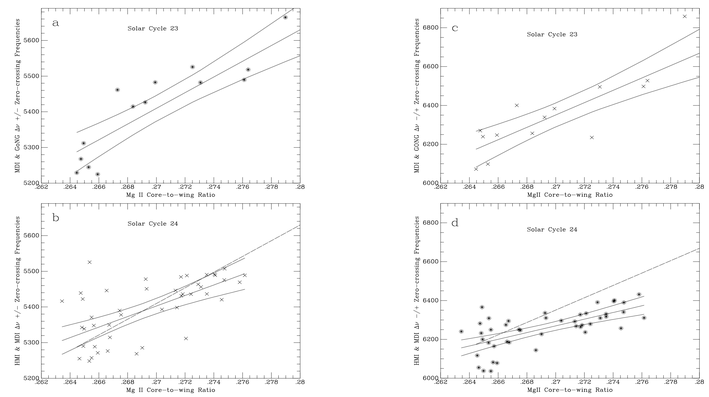

Figure 6: (a) (upper-left): Dependence of the $+/-$ zero-crossing frequencies measured during Cycle 23 as a function of the average MgII Core-to-wing Ratio, an index of solar activity.
(b) (lower-left): Same as panel a except runs from Solar Cycle 24 are shown. The dotted line is the slope from panel a.
(c) (upper-right): Same as panel a except that here the $-/+$ zero-crossing frequency shifts were plotted.
(d) (lower-right): Same as panel c except runs from Solar Cycle 24 are shown. The dotted line is the slope from panel c.
We see statistically-significant differences in the slopes and intercepts of the $-/+$ regression fits at the 99 percent confidence level and of the $+/-$ fits at the 90 percent level.

Conclusions

The signatures of the short-term variations in the frequencies of the solar oscillations were very similar in both Solar Cycles 23 and 24. However, the long-term sensitivity of both sets of zero-crossing frequencies to changes in the MgII activity index was reduced during Cycle 24 by 39 percent from Cycle 23. We believe that this decrease in sensitivity was likely due to structural differences in the solar atmosphere in the two cycles. These results should spur future theoretical analyses of the seismic structure of the solar atmosphere.